Macromolecules

pubs.acs.org/Macromolecules

Article

Preparation of Synthetic Polypeptide–PolyHIPE Hydrogels with Stimuli-Responsive Behavior

Ozgun Can Onder, Petra Utroša, Simon Caserman, Marjetka Podobnik, Ema Žagar, and David Pahovnik*

Cite This: *Macromolecules* 2021, 54, 8321–8330

Read Online

ACCESS | Metrics & More | Article Recommendations | Supporting Information

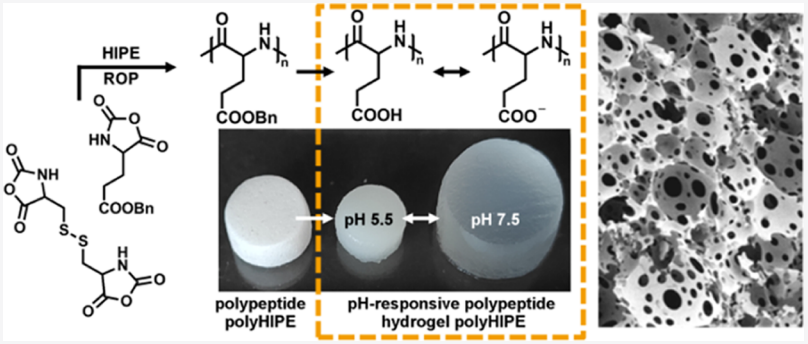

ABSTRACT: In this work, biodegradable macroporous stimuli-responsive polypeptide hydrogels based on L-glutamic acid (Glu) and its copolymers with equimolar amounts of L-phenylalanine (Phe) or L-lysine (Lys) were prepared by deprotection of the corresponding organogels under acidic conditions. The organogels were synthesized by ring-opening polymerization of *N*-carboxyanhydride (NCA) derivatives of the corresponding α-amino acids in oil-in-oil high-internal phase emulsions (HIPEs) using the di-NCA derivative of L-cystine as a cross-linker. The organogels exhibit the typical interconnected porous polyHIPE morphology, which is completely preserved in the hydrogels after removal of the protecting groups of the Glu and Lys repeating units. The pH-dependent behavior and mechanical properties of the obtained hydrogels were studied in buffer solutions with different pH values. At pH 7.5, P(Glu) and P(Glu-*co*-Phe) can be compressed to half their original height and both return to their initial state after unloading. By lowering the pH to 5.5, P(Glu) remains soft, while P(Glu-*co*-Phe) already becomes much stiffer. In contrast, for the P(Glu-*co*-Lys) hydrogel, high buffer uptake was observed only at high or low pH values, whereas at intermediate pH values, the low buffer uptake and the impaired ability to return to the original height are attributed to the attractive ionic interaction between the oppositely charged side groups. We have shown that by tuning the chemical composition of the polypeptides, the uptake, in vitro enzymatic degradation, and compression behavior of the hydrogels can be modulated.

INTRODUCTION

Hydrogels are water-swollen three-dimensional viscoelastic macromolecular networks cross-linked by either covalent bonds or non-covalent interactions. Hydrogels have attracted considerable attention in many fields due to their versatility in terms of composition, preparation, and resulting tunable properties such as swelling ability, interfacial affinity for target substances, response to various stimuli, degradability, viscoelasticity, and network architecture.[1] Polymeric hydrogels have been used as functional materials in a variety of biomedical applications due to their porosity, high water content, and elasticity that resembles biological tissues.[2,3] Biocompatible hydrogels are currently used as prosthetic devices,[4] soft contact lenses,[5] biosensors,[6] surgical dressings,[7] tissue engineering scaffolds,[8] and carriers for therapeutic agents.[9] In addition to physico–chemical properties, another important design criterion for hydrogels to be used in biomedical applications is the network morphology, which is characterized by mesh size, porosity, and connectivity, as these parameters affect the transport properties throughout the hydrogel structure. Typically, the average mesh size of conventional hydrogels is in the range of a few nanometers to a few tens of nanometers, depending on the cross-link density and thus the degree of swelling.[10] This results in a spatial limitation for the transport of molecules larger than the mesh size of the network, which limits the use of hydrogels in macromolecule delivery,[11] bioseparation,[12] and tissue engineering applications.[13,14] To

Received: July 14, 2021
Published: September 10, 2021

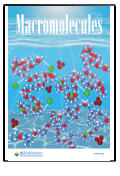

https://doi.org/10.1021/acs.macromol.1c01490
Macromolecules 2021, 54, 8321–8330

overcome these shortcomings, several methods have been developed to prepare macroporous hydrogels, such as porogen leaching,[15] gas foaming,[16] cryogelation,[17] and high-internal phase emulsion (HIPE) templating.[18,19] Among these methods, HIPE templating stands out as it allows the fabrication of macroporous networks with a controlled pore size, porosity, pore structure and volume, and degree of pore interconnectivity.[20] During HIPE templating, gelation of the external phase around the internal-phase droplets takes place. After removal of the internal phase, a highly interconnected pore structure remains, consisting of macroporous voids and interconnecting windows.

Typically, polyHIPE hydrogels are synthesized by polymerizing hydrophilic vinyl or acrylic monomers within the continuous phase of oil-in-water HIPEs. In this way, hydrogels based on styrenesulfonate,[21] 1-vinyl-5-aminotetrazole,[22] acrylamide,[23] acrylic acid,[24] 2-hydroxyethyl methacrylate,[25] *N*-isopropylacrylamide,[26] and amine-functionalized glycidyl methacrylate were prepared.[27] However, their use in biomedical applications is limited due to their non-degradable structure. Biodegradable polyHIPE hydrogels have been prepared using natural polymers, such as alginate[28] and dextran,[29] functionalized with cross-linkable methacrylate groups, or gelatin[30] and chitosan,[31] cross-linked with genipin.

In recent decades, there has been a great deal of interest in the development of stimuli-responsive hydrogels that can rapidly change their structure and volume in a controlled manner depending on environmental temperature, pH, ionic strength, or redox potential.[32,33] A key element in the pH sensitivity of a polymer is the presence of ionizable pendant groups. These groups are capable of exchanging protons in response to changes in the pH of the medium. Hydrogels based on functional synthetic polypeptides are promising biomedical materials because of their innate biodegradability, biocompatibility, and versatile functionality, similar to natural polymers but with better control over their physico-chemical properties.[34] Tailoring the pH-dependent behavior of a given polymer can be achieved by preparing copolymers with other polyelectrolytes or by incorporating hydrophobic moieties into the polymer backbone.[35] Ring-opening polymerization (ROP) of *N*-carboxyanhydrides (NCA) of amino acids provides a suitable approach for the synthesis of polypeptides in scalable amounts, allowing the incorporation of various stimuli-responsive functionalities through monomer selection and/or post-polymerization modification strategies.[36−38] L-Glutamic acid (Glu)-based hydrogels exhibit a pH-dependent phase transition at pH values slightly above their pK_a value due to the presence of ionizable carboxylic acid side groups in the structure[39] and have been used in various biomedical applications.[40,41] Recently, multi-responsive hydrogels or "intelligent" hydrogels have been developed that specifically and uniquely respond to various physiological or externally applied stimuli. By incorporating various stimuli-responsive functionalities into the hydrogel structure, they can mimic the dynamic nature of the native extracellular matrix by undergoing structural changes in response to physiologically benign stimuli. Stimuli-responsive controlled-delivery systems based on intelligent polypeptide hydrogels are also very promising as they can target specific sites and deliver pharmaceutical agents in a localized and sustained manner.[42,43]

Recently, we reported a synthetic strategy to combine NCA chemistry and HIPE templating to prepare hydrophobic polyHIPE organogels based on synthetic polypeptides.[44] In this work, we report the preparation of polyHIPE hydrogels composed entirely of natural amino acids by an organogel-to-hydrogel route. Biodegradable stimuli-responsive polyHIPE hydrogels were prepared from Glu cross-linked with L-cystine and Glu copolymerized with equimolar amounts of L-lysine (Lys) or L-phenylalanine (Phe) to modulate the physico-chemical properties of the hydrogels, such as buffer uptake, compressive properties, and in vitro enzymatic degradation rates.

EXPERIMENTAL SECTION

Materials. γ-Benzyl-L-glutamate (BLG), N^{ε}-carbobenzyloxy-L-lysine (ZLL), and Phe were obtained from Iris Biotech GmbH. Di-*N*-*tert*-butyloxycarbonyl-L-cystine, triphosgene, *N*,*N*-diisopropylethylamine (DIPEA), sodium hydride, iodomethane, sodium thiosulfate, trifluoroacetic acid (TFA), hydrogen bromide (HBr) solution (33 wt % in acetic acid), formic acid, acetic acid, 2-(*N*-morpholino)-ethanesulfonic acid, ethanolamine, tris(hydroxymethyl)-aminomethane, piperidine, 1,4-dithiothreitol (DTT), and protease XIV from *Streptomyces griseus* were obtained from Sigma-Aldrich and used without further purification. Pluronic F127 was purchased from Sigma-Aldrich and was end-group methylated (F127-OMe) as previously published.[45] Petroleum benzine (boiling range 100−140 °C), anhydrous *N*,*N*-dimethylformamide (DMF), dioxane, anhydrous tetrahydrofuran (THF), anhydrous ethyl acetate, *n*-hexane, isopropanol, ethanol, and chloroform were purchased from Merck and used as received.

Synthesis of NCA Monomers. BLG (10 g, 42.2 mmol) was suspended in anhydrous THF (90 mL). The suspension was heated to 50 °C in an oil bath. A solution of triphosgene (6.76 g, 22.8 mmol) in anhydrous THF (10 mL) was then added dropwise under argon. The mixture was stirred at 50 °C under argon for 2 h to give a clear solution. The mixture was concentrated under a vacuum, and the product was precipitated from *n*-hexane and placed in a freezer overnight. The filtered product was recrystallized three times from THF/*n*-hexane. BLG NCA was obtained in the form of a white powder (9.57 g, 86% yield). The ^{1}H and ^{13}C NMR spectra with signal assignation are shown in Figure S1.

Di-*N*-*tert*-butyloxycarbonyl-L-cystine (1 g, 2.3 mmol) was suspended in anhydrous ethyl acetate (15 mL). Triphosgene (0.91 g, 3.1 mmol) was then added in one portion at room temperature. The mixture was heated to 60 °C in an oil bath and stirred at this temperature under argon for 12 h. The mixture was then filtered through a syringe filter (0.45 μm, PTFE, Aldrich) in a centrifuge tube (50 mL) containing 40 mL of *n*-hexane. After centrifugation at 8000 rpm for 7 min, the supernatant was decanted. The product was dried in a desiccator and further purified by repeating the precipitation twice. L-Cystine NCA was obtained in the form of a white powder (0.58 g, 83% yield). The ^{1}H and ^{13}C NMR spectra with signal assignation are shown in Figure S2.

ZLL (10 g, 35.7 mmol) was suspended in anhydrous ethyl acetate (90 mL). The suspension was heated to 78 °C in an oil bath. A solution of triphosgene (4.70 g, 15.9 mmol) in anhydrous ethyl acetate (10 mL) was then added dropwise to the suspension under argon. The mixture was stirred at 78 °C under argon for 4 h to give a clear solution. The mixture was concentrated under a vacuum, and the product was precipitated from *n*-hexane and placed in a freezer overnight. The filtered product was recrystallized three times from the THF/*n*-hexane. ZLL NCA was obtained in the form of a white powder (7.65 g, 70% yield). The ^{1}H and ^{13}C NMR spectra with signal assignation are shown in Figure S3.

Phe (2 g, 12.1 mmol) was suspended in anhydrous THF (20 mL). The suspension was heated to 50 °C in an oil bath. A solution of triphosgene (1.38 g, 4.7 mmol) in anhydrous THF (10 mL) was then added dropwise to the suspension under argon. The mixture was stirred at 50 °C under argon for 3 h to give a clear solution. The mixture was concentrated under a vacuum, and the product was precipitated from *n*-hexane and placed in a freezer overnight. The

https://doi.org/10.1021/acs.macromol.1c01490
Macromolecules 2021, 54, 8321−8330

filtered product was recrystallized three times from the THF/*n*-hexane. Phe NCA was obtained in the form of a white powder (1.39 g, 60% yield). The ^{1}H and ^{13}C NMR spectra with signal assignation are shown in Figure S4.

HIPE Templating. The experimental conditions for the preparation of oil-in-oil emulsions are given in Table S1. The external phase was prepared by successively dissolving the surfactant (F127-OMe), the monomer(s), and the cross-linker in anhydrous DMF at room temperature in a three-necked round-bottom flask equipped with an overhead stirrer, an addition funnel, and a rubber septum through which argon gas was introduced. With mechanical stirring of the external phase at 330 rpm, the internal phase (petroleum benzine) was added dropwise at a rate of 0.5 mL/min. After completion of petroleum benzine addition, stirring was continued for another 10 min, and then, the catalyst solution (0.5 M DIPEA in DMF) was added in one portion. Stirring was continued for an additional 30 s to ensure uniform dispersion of the catalyst. The emulsion was then aliquoted into 2 mL polypropylene Eppendorf tubes using an automatic pipette and sealed with septum caps. A needle was then inserted into each cap to allow release of CO_2 generated in situ during ROP. The emulsions were polymerized at room temperature for 24 h. The resulting gels were purified by Soxhlet extraction with dioxane for 48 h and then freeze-dried. The polymerization yield of polyHIPEs was determined gravimetrically according to eq 1, where m_{polyHIPE} is the total mass of the purified and dried polyHIPE, m_{NCA} is the total mass of all NCAs used for HIPE preparation, and m_{CO2} is the calculated mass of CO_2 released by assuming 100% monomer conversion.

$$\text{Yield}\ (\%) = \frac{m_{\text{polyHIPE}}}{m_{\text{NCA}} - m_{\text{CO}_2}} \times 100 \tag{1}$$

The total porosity was measured gravimetrically according to eq 2, where the monolith density (d_{monolith}) was determined from the weight and volume of the polyHIPE. For polymer densities (d_{polymer}), the literature value of PBLG (1.28 g/cm^3) was used.[46]

$$\text{Porosity}\ (\%) = \left(1 - \frac{d_{\text{monolith}}}{d_{\text{polymer}}}\right) \times 100 \tag{2}$$

Hydrogel Preparation. 4 mL of TFA and 0.3 mL of HBr solution were added in a glass vial and stirred. 40 mg of polyHIPE piece was immersed in this solution for 2 h at 4 °C. Then, the polyHIPE was transferred to 10 mL of THF for 10 min, which was replaced three times, each time leaving the sample in fresh 10 mL of solvent for 1 h. The sample was then placed in 10 mL of buffer with pH 7.5 for 24 h, which was exchanged three times. Finally, the P(Glu) and P(Glu-*co*-Phe) hydrogels were placed in a buffer of pH 4.0, while the P(Glu-*co*-Lys) hydrogels were placed in a buffer of pH 6.5 for 24 h. Afterward, the hydrogels were immersed in distilled water to remove buffer salts, freeze-dried, and stored in a desiccator. For morphological characterization of the deprotected hydrogels, the gels were instead immersed in dioxane and freeze-dried after three dioxane exchanges.

Preparation of Buffer Solutions. Formic acid (3.0, 3.5, and 4.0), acetic acid (4.5 and 5.0), 2-(*N*-morpholino) ethanesulfonic acid (5.5 and 6.5), tris(hydroxymethyl) aminomethane (Tris) (7.5 and 8.5), ethanolamine (9.0, 9.5, and 10.0), and piperidine (10.5 and 11.0) were used to prepare buffer solutions with pH values indicated in parentheses. To prepare 1 L of buffer solution, an appropriate buffer was first dissolved in 800 mL of distilled water at room temperature to obtain a final 0.125 M buffer solution. The solution was then titrated with 1.0 M HCl or NaOH to obtain the desired pH. The ionic strength of the buffer solution was calculated and the required amount of NaCl was added to the buffer solution to obtain a final ionic strength of 0.15 M. The volume was then increased to 1 L in a volumetric flask by adding distilled water. Buffer with pH 7.5 and 0.05 M ionic strength was prepared by diluting the original pH 7.5 buffer three times. Buffer with pH 7.5 and 0.45 M ionic strength was prepared by dissolving a sufficient amount of NaCl in the original 7.5 pH buffer.

Buffer Uptake. The pH-dependent behavior of the hydrogels was studied by measuring the uptake in buffers with different pH values. Accordingly, hydrogel pieces were placed in buffers, and the pieces were removed at appropriate time intervals until no change in weight with time was observed. Before weighing the swollen sample, any surface water was removed with filter paper. The buffer uptake was calculated according to eq 3, where W_{d} and W_{s} denote the weight of dry and swollen hydrogel, respectively.

$$\text{Buffer uptake} = \frac{W_{\text{s}} - W_{\text{d}}}{W_{\text{d}}} \tag{3}$$

Characterization. ^{1}H NMR spectra were recorded at 25 °C in deuterated dimethyl sulfoxide (DMSO-d_6) using a Varian Unity Inova 300 MHz spectrometer (Varian, USA) in the pulse Fourier transform mode. Chemical shifts are expressed as δ and ppm relative to tetramethylsilane (δ = 0). The morphology of the monoliths was studied by scanning electron microscopy (SEM) on a high-resolution SEM Zeiss Ultra plus instrument (Carl Zeiss, Germany). The samples were broken with a razor blade after immersion in liquid nitrogen. For charge dissipation during SEM analysis, the obtained cross-sections were coated with a 10 nm-thick gold layer using a Gatan PECS 682 (Gatan, USA). Pore size analyses were performed with ImageJ software, using a correction factor of $2/(3^{0.5})$ to compensate for statistical error.[47] Fourier-transform infrared spectroscopy (FTIR) spectra were acquired using a Spectrum One FTIR spectrometer (PerkinElmer, U.K.). FTIR spectra were recorded in an attenuated total reflectance mode in a spectral range of 650−4000 cm^{-1}.

Mechanical Testing. The compressive mechanical properties of the hydrogel samples were measured using a DMA Q800 dynamic mechanical analyzer (TA Instruments) and 40 mm-diameter compression disks. The polyHIPEs were first cut into slices of uniform size, with a cross-sectional diameter of ∼7 mm and a height of ∼5 mm. After deprotection and equilibration in buffer at pH 7.5 or 5.5 (ionic strength of 0.15 M, unless otherwise specified), the diameter of the hydrogel disks varied depending on the buffer uptake, which was taken into account in the calculations and in setting the compression rate. Excess surface water was removed from the hydrogels with filter paper prior to measurements. All uniaxial compression-strain measurements were performed at 37 °C. Mass loss of the specimens due to water evaporation during the measurements was negligible.

A preload force was applied to ensure complete contact between the plate surface and the specimen. The hydrogels were gradually compressed to 50% strain within 10 min and then unloaded at the same rate to the preload force. The compressive Young's moduli (E) of the specimens were determined from the slope of the initial linear region of the loading stress−strain curve. The final strain of the specimen (ε_{f}) after unloading was recorded within 3 min. The height recovery was calculated according to eq 4.

$$\text{Height recovery}\ (\%) = (1 - \varepsilon_{\text{f}}) \times 100 \tag{4}$$

The hysteresis energy of the cycle was estimated by calculating the area between the loading and unloading curves. At least two specimens of each sample were measured.

Reductive Degradation of Hydrogels. 10 mg pieces of the dried hydrogels were soaked in 1 mL of D_2O containing 0.025 M DTT and 0.025 M sodium carbonate (pH 11.3). The soaked samples were kept at 37 °C, and the decomposition of the hydrogels was observed by visual evaluation. After complete dissolution of the hydrogels, ^{1}H NMR spectra of the solutions were recorded to determine their chemical composition.

Enzymatic Degradation of Hydrogels. Enzymatic degradation assays were performed using protease XIV from *S. griseus* (specific activity: 3.5 U/mg protein) according to previously reported procedures.[48] First, purified and freeze-dried hydrogel samples (10 mg dry weight) were soaked in pH 7.5 buffer (0.125 M Tris and 0.15 M ionic strength) to obtain swollen hydrogels. After reaching uptake equilibrium, the hydrogel samples were transferred to protease type XIV solution (2 mL and 0.01 U/mL) and incubated at 37 °C. The

https://doi.org/10.1021/acs.macromol.1c01490
Macromolecules 2021, 54, 8321−8330

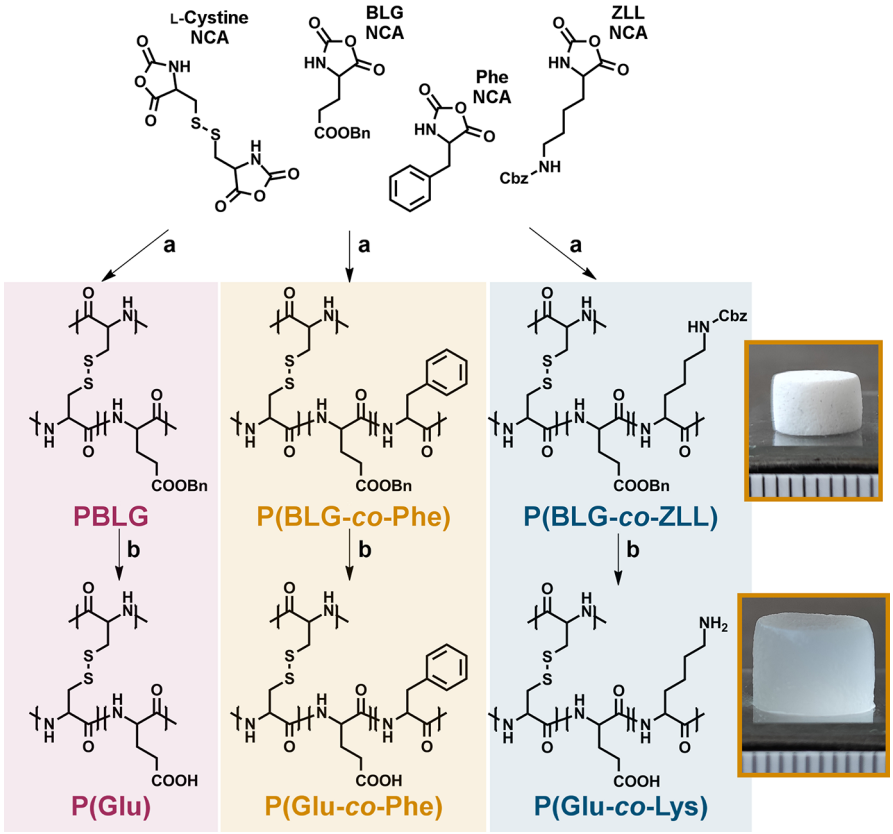

Figure 1. Schematic representation of the preparation of macroporous polypeptide hydrogels by (a) ROP of NCA in the continuous phase of HIPE, catalyzed with DIPEA and (b) followed by deprotection of the organogels in HBr/TFA. The photographs on the right show dry P(BLG-*co*-Phe, top) and swollen P(Glu-*co*-Phe, bottom) at pH 7.5 (scale interval 1 mm).

enzyme solution contained 5 mM $CaCl_2$ to prevent autolysis. During analysis, the enzyme solution was changed daily to maintain enzyme activity. At specific time points, samples were removed and immersed in 10 mL of pH 7.5 buffer at 4 °C to remove the enzyme solution. To ensure complete removal, 10 mL of buffer was replaced three times at 4 °C within 24 h. Then, the buffer solution of the partially degraded P(Glu), P(Glu-*co*-Phe), and P(Glu-*co*-Lys) hydrogel samples was exchanged with pH 4.0, 4.0, and 5.5 buffers, respectively. After the hydrogels reached uptake equilibrium, they were immersed in distilled water, which was replaced three times to remove the buffer salts. Then, the samples were freeze-dried and weighed. The weight percentage of the degraded hydrogels was calculated according to eq 5, where W_i is the initial weight of the dried hydrogel piece and W_f is the final weight of the dried hydrogel piece after enzymatic degradation. Each assay was performed in triplicate. For P(Glu-*co*-Lys) samples, enzymatic degradation was also assayed in 0.25 U/mL protease solutions using the same procedure. In addition, control experiments were performed using an identical procedure by incubating hydrogels with pH 7.5 buffer and 5 mM $CaCl_2$, without enzyme.

$$\text{Weight fraction (\%)} = \frac{W_f}{W_i} \times 100 \quad (5)$$

Toxicity Assay. Hydrogel samples (20 mg) were soaked overnight in absolute ethanol to sterilize them. The next day, the ethanol was replaced with sterile Milli-Q water. One day before the cell toxicity experiment, the hydrogel samples were washed for 15 min in colorless test medium [DMEM D5921 supplemented with 10% v/v FBS, 1% v/v Na-Pyruvate S8636 (both from Sigma-Aldrich), and with 1% v/v Glutamax 35 050 061 (from Gibco)]. The hydrogel samples were then transferred to separate wells of a 12-well cell culture plate in 1 mL of test medium and incubated overnight in a cell culture incubator under normal conditions (5% CO_2, 37 °C, and near 100% humidity). One day before the experiment, the mouse fibrosarcoma cell line L929 was seeded in a white 96-well microtiter plate (Costar 3610) at a density of 10,000 cells per well in 100 μL of test medium and incubated overnight in a cell culture incubator. The next day, 100 μL of the medium incubated in the presence and absence of the hydrogels was transferred to the cells in the microtiter plate as a treatment and control, respectively. The cells were incubated in the cell culture incubator for another day. Then, 20 μL of Presto Blue cell viability reagent (Invitrogen) was added to the wells, and the plates were incubated for another 3 h to allow the live cells to form a fluorescent product. The signal was measured with a plate reader using an excitation filter at 570 nm and an emission filter at 590 nm. The viability signal of the cells in the polymer-conditioned medium was expressed as a percentage of the control. The experiment was repeated three times.

RESULTS AND DISCUSSION

Due to the sensitivity of the ROP of NCA to the presence of water, we chose an organogel-to-hydrogel route to prepare polypeptide−polyHIPE hydrogels (Figure 1). In our recent study, we developed a method for preparation of polypeptide−polyHIPE organogels via ROP of NCA monomers in oil-in-oil emulsions.[44] Using this approach, we have here prepared redox-responsive PBLG as well as P(BLG-*co*-Phe) and P(BLG-*co*-ZLL) copolypeptide polyHIPEs using equimolar amounts of L-phenylalanine(Phe)- or L-lysine(Lys)-based monomers to study the effect of incorporating hydrophobic or amine groups into the hydrogel structure on their stimuli-responsive behavior. A di-NCA derivative of L-cystine containing a disulfide bond in the structure was used as a cross-linker.

https://doi.org/10.1021/acs.macromol.1c01490
Macromolecules 2021, 54, 8321−8330

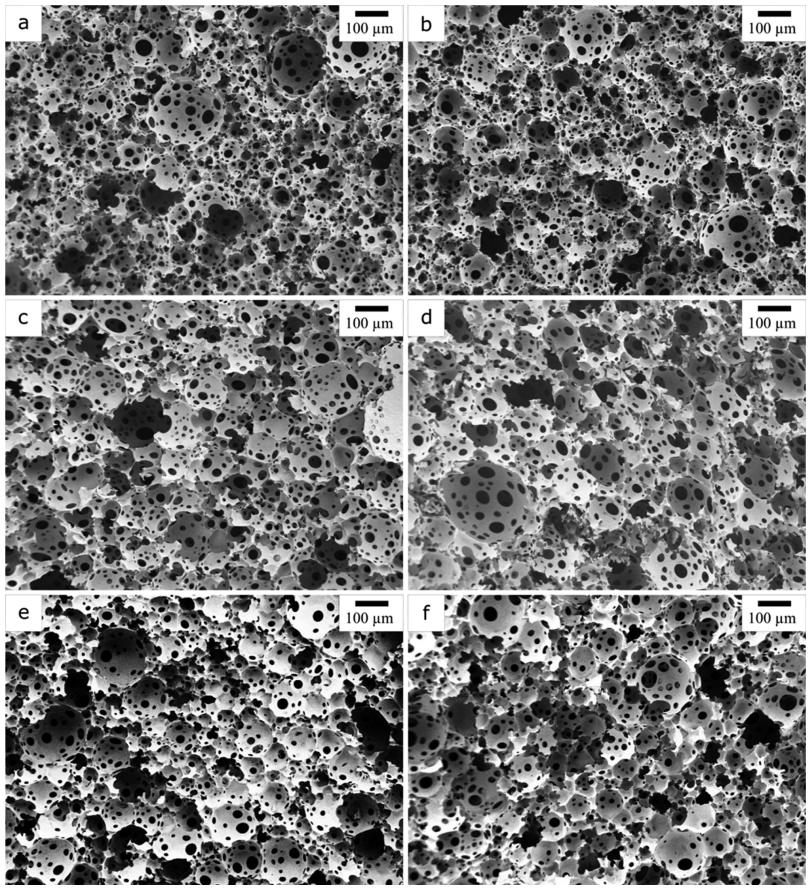

Figure 2. SEM cross-section images of polyHIPEs, which were freeze-dried from dioxane before and after removal of protecting groups. (a) PBLG, (b) P(Glu), (c) P(BLG-*co*-Phe), (d) P(Glu-*co*-Phe), (e) P(BLG-*co*-ZLL), and (f) P(Glu-*co*-Lys).

The formulations used to prepare the corresponding polyHIPEs are shown in Table S1.

ROP of NCA was carried out by an activated monomer mechanism using an appropriate amount of DIPEA as the catalyst to ensure rapid gelation of the external phase while avoiding foaming of HIPE. For PBLG and P(BLG-*co*-Phe) polyHIPEs, 0.5 mol % catalyst was used, while for P(BLG-*co*-ZLL), 1.0 mol % was used due to the slower polymerization rate of ZLL NCA. For all samples, 80 vol % HIPE internal phase (petroleum benzine) and 5 mol % cross-linker were used. The obtained polyHIPE organogels were purified by Soxhlet extraction with dioxane to remove the solvents, surfactant, and any soluble polymer chains that were not part of the polyHIPE network.

The organogels were converted to hydrogels by removing the benzyl protecting groups from PBLG and PZLL with dry HBr in acetic acid.[49] To optimize the time required for complete removal of the benzyl protecting groups while avoiding significant degradation of the peptide bonds and thus disintegration of the network,[50] a series of polyHIPEs were simultaneously immersed in HBr solution in TFA. After every 30 min, one of the specimens was removed and immersed in THF to remove most of the deprotection agents from the polyHIPE. This step was crucial because when we attempted to remove the deprotection agents directly with aqueous solutions, extensive hydrolysis of the peptide bonds in the polyHIPE network was observed. After we removed the excess HBr from the gels, the S−S bonds of the cross-linker in the structure of the gels were cleaved by reduction with DTT in D_2O, taking advantage of the redox sensitivity of the networks. This allowed us to analyze the resulting water-soluble polypeptide chains by ^{1}H NMR. It was found that deprotection of the organogels with HBr for 2 h was sufficient to completely remove the benzyl protecting groups, as indicated by tracking the disappearance of the benzyl proton signals with deprotection time. The successful deprotection of the polypeptide networks was also confirmed by FTIR spectroscopy by the disappearance of the carbonyl band of the benzyl protecting groups at ∼1725 cm^{-1} (Figures S5−S7). In addition, from the ^{1}H NMR spectra of the reduced samples, the chemical composition of the hydrogels was determined by integrating the characteristic amino acid signals (Figures S8−S10). Glu/Phe and Glu/Lys ratios of 1.06 and 1.08, respectively, were determined, which are in good agreement with the targeted chemical compositions of the corresponding polypeptide networks.

Cross-sectional images of the freeze-dried organogels show a highly interconnected porous structure for all samples, consisting of voids and interconnected windows, which are typical of the polyHIPE morphology (Figure 2). The average pore size, porosity, and yields of the polyHIPEs are listed in Table 1, and the pore size distribution can be seen in Figure S11. Importantly, the shape of the samples and the typical polyHIPE morphology, as shown by SEM in Figure 2, are fully preserved after removal of the protecting groups of the polypeptide networks. The resulting deprotected hydrogels were then soaked in aqueous buffer solutions to obtain hydrogels with different degrees of buffer uptake, depending on

https://doi.org/10.1021/acs.macromol.1c01490
Macromolecules 2021, 54, 8321−8330

Table 1. Properties of the polyHIPEs

	PBLG	P(BLG-*co*-Phe)	P(BLG-*co*-ZLL)
yield (%)	85.5	88.3	74.8
average void size (μm)	59 ± 31	61 ± 32	56 ± 30
density (g/cm^3)	0.12 ± 0.01	0.13 ± 0.01	0.13 ± 0.01
porosity (%)	90.6 ± 1.1	89.8 ± 0.8	89.5 ± 0.9
catalyst amount (mol %)	0.5	0.5	1.0

their chemical composition and the pH/ionic strength of the solutions.

To investigate the effect of pH on buffer uptake, the hydrogels were soaked in buffer solutions with different pH values, while the ionic strength was adjusted to 0.15 M by adding NaCl. In the case of P(Glu), it was observed that the buffer uptake of the hydrogel increased with pH, which is attributed to the increasing degree of ionization of the carboxyl groups and the associated electrostatic repulsions between the negatively charged carboxylate groups (Figure 3a).[35] A significant increase in uptake was observed between pH 4 and 5.5, after which it began to level off. This is expected because the carboxyl groups of P(Glu) have a pK_a of 4.36,[51] so by pH 5.5, most of them are already in their deprotonated state. The P(Glu)-hydrogel shows a reversible swelling behavior with fully preserved shape upon pH change. The uptake of the P(Glu-*co*-Phe) hydrogel also increases with increasing pH of the medium. However, due to the incorporation of Phe amino acids into the network structure, the hydrophobic interactions in aqueous solution lead to lower uptake values of P(Glu-*co*-Phe) compared to P(Glu) hydrogel. Moreover, the transition pH shifts to a slightly higher value due to the stronger electrostatic repulsion required to swell the P(Glu-*co*-Phe) network (Figure 3b).[52] In contrast, copolymerization of Glu with Lys results in a hydrogel that exhibits low buffer uptake when the pH is between the pK_a values of the pendant carboxyl groups of P(Glu) (4.36) and the amino groups of P(Lys) (9.29),[51] which is due to the attractive Coulomb interactions of the oppositely charged pendant groups. Higher uptakes of P(Glu-*co*-Lys) were observed only in buffer solutions with very low or very high pH values, where the gel network began to accumulate either net positive or net negative charge (Figure 3c).

The differences between the polyHIPE hydrogels of different chemical compositions were further studied with mechanical compression tests at pH values of 7.5 and 5.5. During loading, the hydrogels were gradually compressed to a strain of 50% within 10 min, which is sufficient to observe the elastic and plastic deformations of the specimens. The loading was followed by an unloading phase at the same rate, during which the ability of the hydrogels to return to their initial height was studied. All hydrogels exhibited a typical foam compression behavior with an initial linear elastic region followed by a stress plateau region and finally a densification region associated with a more rapid increase in stress at higher strains (Figures 4 and S12).[53]

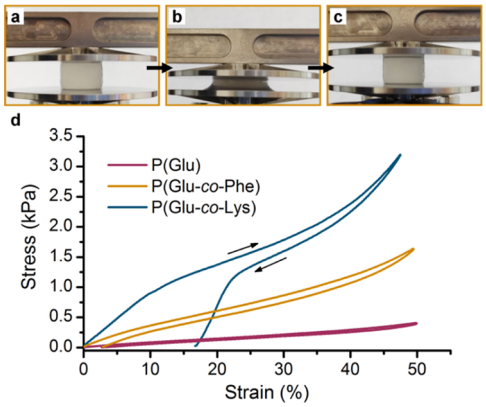

Figure 4. Photographs of polyHIPE hydrogel P(Glu-*co*-Phe) (a) before compression, (b) compressed to 50% of initial height, and (c) after compression and (d) stress–strain curves of compressive loading and unloading of polyHIPE hydrogels at 37 °C and pH 7.5. Arrows indicate the direction of the process.

To evaluate the stiffness of the hydrogels, Young's moduli were determined from the stress–strain curves (Table 2). The values of the moduli correlate with the solid content of the hydrogels, which is a direct consequence of the uptake and degree of swelling of the material, as previously documented in the literature.[54] The P(Glu) hydrogel has the highest water content and is therefore the softest with a low modulus of 0.78 kPa. However, the covalent cross-links maintain its mechanical integrity, and the hydrogel withstands compression without breaking. Compared to P(Glu), the P(Glu-*co*-Phe) uptakes buffer to a lesser extent, its ability to resist deformation is improved, and finally a higher value of modulus (3.50 kPa) was observed. In the P(Glu-*co*-Lys) hydrogel, the attractive electrostatic Coulomb interactions between the negatively and positively charged groups act as additional physical cross-

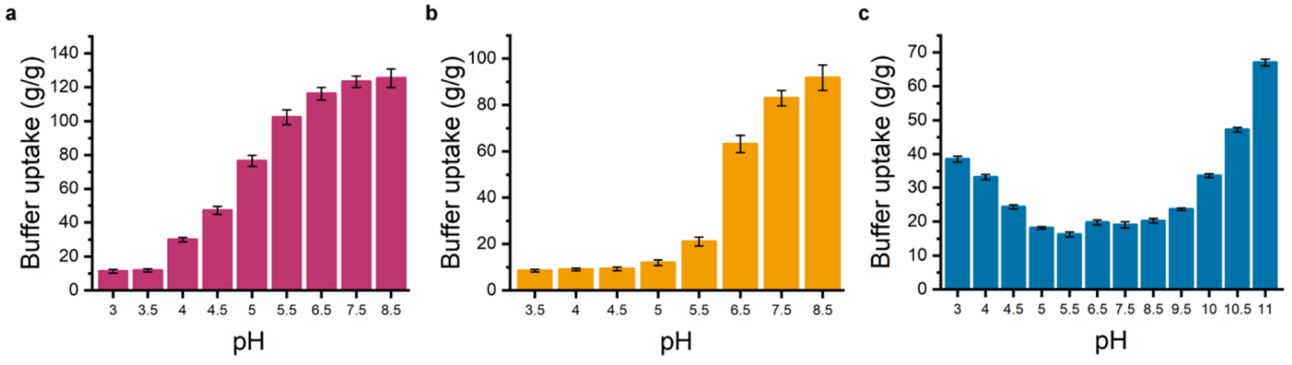

Figure 3. Buffer uptake of (a) P(Glu), (b) P(Glu-*co*-Phe), and (c) P(Glu-*co*-Lys) hydrogels as a function of medium pH. For each sample, average values of three specimens with standard errors are shown.

https://doi.org/10.1021/acs.macromol.1c01490
Macromolecules 2021, 54, 8321–8330

Table 2. Mechanical Properties [Compressive Modulus (E), Height Recovery (R) and Hysteresis Energy] of Hydrogel-polyHIPEs at Different pH Values Determined from Compressive Loading−Unloading Tests at 37 °C

polyHIPE	pH	E (kPa)	R (%)	hysteresis energy (kJ/m^3)
P(Glu)	7.5	0.78 ± 0.18	97.3 ± 0.1	1.7 ± 0.4
	5.5	0.74 ± 0.05	97.7 ± 0.6	1.8 ± 0.4
P(Glu-*co*-Phe)	7.5	3.50 ± 0.56	97.5 ± 0.6	4.9 ± 0.4
	5.5	122 ± 19	65.8 ± 6.5	750 ± 310
P(Glu-*co*-Lys)	7.5	8.72 ± 0.43	83.8 ± 1.4	26.8 ± 7.9
	5.5	9.1 ± 2.1	88.1 ± 5.1	21.9 ± 7.4

links, resulting in the least swollen hydrogel with the highest modulus of 8.72 kPa.

During compression, water is squeezed out of the hydrogels. When the hydrogels are gradually released by continuously decreasing the applied force until only the initial preload force is reached, the squeezed-out water is reabsorbed and the hydrogels recover their original shape (Figures 4 and S13). The recovered shapes were achieved within 3 min after unloading. Both P(Glu) and P(Glu-*co*-Phe) show an excellent height recovery of more than 97.0% and a small hysteresis area between the loading and unloading curves, corresponding to the dissipated energy.[55] The compression could be repeated several times without showing any damage to the samples. P(Glu-*co*-Lys), on the other hand, recovered only to 83.8% of its original height and shows a pronounced hysteresis probably due to a reversible disassembly and reassembly of the physical cross-links.[56,57] This effect is more pronounced at slower loading and unloading rates as this gave the physical network more time to rearrange. On the other hand, P(Glu-*co*-Lys) shows a similar unloading behavior as P(Glu) and P(Glu-*co*-Phe) when a higher compression rate is used. Namely, after slow (20 min) loading and unloading, the height recovery is 72.5%, while after fast (5 min) loading and unloading, the recovery reaches 94.9%, compared to 83.8% when each step takes 10 min. Changing the compression rate has no significant effect on the unloading behavior of P(Glu) and P(Glu-*co*-Phe). Moreover, the height recovery of P(Glu-*co*-Lys) improves to 90.1% and the hysteresis area decreases when the hydrogel is soaked in buffer with higher ionic strength (0.45 M) and compressed, whereby higher buffer uptake was observed (Figure S14). The additional ions may help to partially shield the attractive forces between the positively and negatively charged side groups, leading to the disruption of the physical cross-links and finally to a higher degree of network swelling,[58] which is known as the anti-polyelectrolyte effect.[59] A similar anti-polyelectrolyte behavior was observed in polyHIPEs prepared from a zwitterionic acrylate-based monomer.[60] On the other hand, P(Glu) and P(Glu-*co*-Phe) show the typical polyelectrolyte effect. Namely, as the salt concentration increases, the repulsive forces between the negatively charged ions decrease due to the shielding of the ionic groups, which typically leads to lower degrees of swelling and buffer uptake (Figure S14).[59]

Lowering the pH from 7.5 to 5.5 only slightly affects the buffer uptake of the P(Glu) and P(Glu-*co*-Lys) hydrogels, so their mechanical properties do not change significantly (Table 2 and Figure S15). Compared to pH 7.5, P(Glu-*co*-Phe) uptakes significantly less buffer at pH 5.5, where the uptake is comparable to that of P(Glu-*co*-Lys). However, P(Glu-*co*-Lys) remains soft, whereas the P(Glu-*co*-Phe) becomes much stiffer at pH 5.5, as shown by a ∼35-fold increase in modulus (Table 2). P(Glu-*co*-Phe) at pH 5.5 recovers only part of its original height after compression, even after a longer recovery time (15 min), indicating permanent deformation.[61]

To analyze the enzymatic degradation of hydrogels, we used protease type XIV, which is a mixture of different endopeptidases, exopeptidases, and caseinolytic enzymes produced by *S. griseus*.[62] Because of its similarity to mammalian proteases,[63,64] it has often been used as a model enzyme mixture to study the complete enzymatic degradation behavior of polypeptide-based hydrogel systems in vitro.[65,66] The degradation profile of hydrogels in protease solutions at pH 7.5 and 37 °C is shown in Figure 5. In 0.01 U/mL protease solutions, P(Glu) and P(Glu-*co*-Phe) hydrogels were completely degraded within 3 and 4 days, respectively. After complete degradation, clear solutions without any residue were obtained. However, the degradation of P(Glu-*co*-Lys) hydrogel was slower in 0.01 U/mL protease solution, and degradation of about 30% was observed after 6 days. At pH 7.5, the P(Glu) and P(Glu-*co*-Phe) hydrogels are in a highly swollen state, allowing the protease molecules to easily reach the peptide bonds and the soluble degradation products to diffuse out of the network, leading to a gradual decrease in the weight of the hydrogels and finally to the complete disintegration of the network. The P(Glu-*co*-Phe) hydrogel degrades slightly slower than the P(Glu) hydrogel most likely due to the presence of hydrophobic Phe residues, which reduce the solubility of the degradation products after random cleavage and require a higher degree of degradation to fully dissolve. Much slower degradation was observed for the P(Glu-*co*-Lys) hydrogel, which can be attributed to the presence of physical cross-links in addition to the covalent cross-links. Due to this additional cross-linking, degradation must reach a higher degree to result in degradation products that are soluble in the buffer at pH 7.5. When the P(Glu-*co*-Lys) hydrogel was exposed to a higher protease concentration (0.25 U/mL), the degradation rate was significantly increased and the hydrogel was completely dissolved within 4 days. After degradation, clear solutions without residues were obtained. In control buffer solutions with a pH of 7.5 and containing 5 mM $CaCl_2$ in the absence of

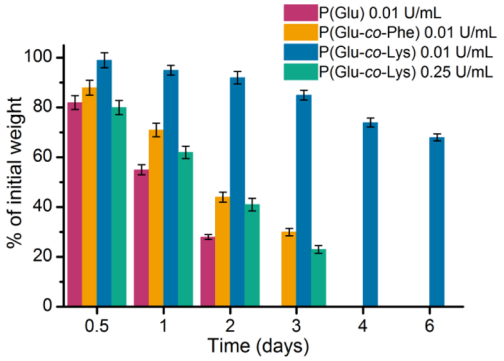

Figure 5. Enzymatic degradation profiles of P(Glu), P(Glu-*co*-Phe), and P(Glu-*co*-Lys) hydrogels in 0.01 U/mL protease type XIV solutions at pH 7.5 and 37 °C. P(Glu-*co*-Lys) hydrogels were also degraded in 0.25 U/mL protease type XIV solution under the same conditions. For each sample, average values of three specimens with standard errors are shown.

https://doi.org/10.1021/acs.macromol.1c01490
Macromolecules 2021, 54, 8321−8330

the enzyme mixture, no degradation of the samples was observed after 2 weeks.

Because these macroporous stimuli-responsive hydrogels are potential candidates for various biomedical applications, the biocompatibility of the hydrogels was evaluated by cytotoxicity analysis. After deprotection of the hydrogels, the obtained samples were purified by multiple solvent exchanges. The absence of by-products was already confirmed by ^{1}H NMR of the reductively degraded hydrogels. The absence of toxic residues in the material was also confirmed by cell viability experiments, where the hydrogel samples were soaked in a medium for 24 h. This medium was then transferred to the L929 mouse fibrosarcoma cell culture. The hydrogels were found to be non-cytotoxic as no reduction in cell viability was observed as shown by the comparable viability signals of the treated cultures and the control in Figure 6.

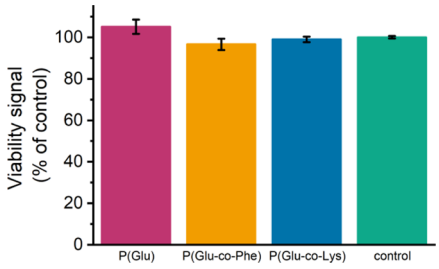

Figure 6. Viability assay of L929 cells treated with medium incubated overnight with hydrogels or without them (control). For each sample, average values of three specimens with standard errors are shown.

CONCLUSIONS

Polypeptide−polyHIPE hydrogels were prepared via an organogel-to-hydrogel route. PBLG, P(BLG-*co*-Phe), and P(BLG-*co*-ZLL) polyHIPEs were synthesized in oil-in-oil emulsions with 5 mol % L-cystine as the cross-linker. After deprotection under acidic conditions, P(Glu), P(Glu-*co*-Phe), and P(Glu-*co*-Lys) hydrogels were obtained, which show fully preserved shape and polyHIPE morphology. The hydrogels can be degraded by reduction of disulfide bonds or enzymatically. Because the hydrogels contain ionizable pendant groups, they exhibit buffer uptake and a compression behavior depending on the pH and ionic strength of the medium and can be modulated by tuning the chemical composition of the polypeptides. The buffer uptake of both P(Glu) and P(Glu-*co*-Phe) hydrogels increases with increasing medium pH. Compared to P(Glu) hydrogel, the transition of P(Glu-*co*-Phe) shifts to higher pH due to the hydrophobic interactions present in P(Glu-*co*-Phe). At pH 7.5, both hydrogels can be compressed to half their original height and they return to their initial state after unloading, whereas P(Glu-*co*-Phe) becomes much stiffer at pH 5.5. In contrast, the P(Glu-*co*-Lys) hydrogel has a high uptake only in buffers with pH values below 4 and above 9. At intermediate pH values, the low buffer uptake and impaired ability to return to the original height are attributed to the attractive ionic interactions between the oppositely charged side groups in the P(Glu-*co*-Lys), which cause additional physical cross-linking.

ASSOCIATED CONTENT

Supporting Information

The Supporting Information is available free of charge at https://pubs.acs.org/doi/10.1021/acs.macromol.1c01490.

^{1}H and ^{13}C NMR spectra, FTIR spectra, pore size distribution, buffer uptake, and mechanical behavior (PDF)

AUTHOR INFORMATION

Corresponding Author

David Pahovnik − *Department of Polymer Chemistry and Technology, National Institute of Chemistry, 1000 Ljubljana, Slovenia;* orcid.org/0000-0001-8024-8871; Email: david.pahovnik@ki.si

Authors

Ozgun Can Onder − *Department of Polymer Chemistry and Technology, National Institute of Chemistry, 1000 Ljubljana, Slovenia*

Petra Utroša − *Department of Polymer Chemistry and Technology, National Institute of Chemistry, 1000 Ljubljana, Slovenia*

Simon Caserman − *Department of Molecular Biology and Nanobiotechnology, National Institute of Chemistry, 1000 Ljubljana, Slovenia*

Marjetka Podobnik − *Department of Molecular Biology and Nanobiotechnology, National Institute of Chemistry, 1000 Ljubljana, Slovenia*

Ema Žagar − *Department of Polymer Chemistry and Technology, National Institute of Chemistry, 1000 Ljubljana, Slovenia;* orcid.org/0000-0002-2694-4312

Complete contact information is available at: https://pubs.acs.org/10.1021/acs.macromol.1c01490

Notes

The authors declare no competing financial interest.

ACKNOWLEDGMENTS

The authors acknowledge the financial support from the Slovenian Research Agency (research core funding no. P2-0145 and projects nos. J2-9214 and N2-0131).

REFERENCES

(1) Ahmed, E. M. Hydrogel: Preparation, Characterization, and Applications: A Review. *J. Adv. Res.* **2015**, *6*, 105−121.

(2) Peppas, N. A.; Keys, K. B.; Torres-Lugo, M.; Lowman, A. M. Poly(Ethylene Glycol)-Containing Hydrogels in Drug Delivery. *J. Controlled Release* **1999**, *62*, 81−87.

(3) Saha, N.; Saarai, A.; Roy, N.; Kitano, T.; Saha, P. Polymeric Biomaterial Based Hydrogels for Biomedical Applications. *J. Biomater. Nanobiotechnol.* **2011**, *02*, 85−90.

(4) Guiseppi-Elie, A. Electroconductive Hydrogels: Synthesis, Characterization and Biomedical Applications. *Biomaterials* **2010**, *31*, 2701−2716.

(5) Hu, X.; Hao, L.; Wang, H.; Yang, X.; Zhang, G.; Wang, G.; Zhang, X. Hydrogel Contact Lens for Extended Delivery of Ophthalmic Drugs. *Int. J. Polym. Sci.* **2011**, *2011*, 814163.

(6) Mateescu, A.; Wang, Y.; Dostalek, J.; Jonas, U. Thin Hydrogel Films for Optical Biosensor Applications. *Membranes* **2012**, *2*, 40−69.

(7) Balakrishnan, B.; Mohanty, M.; Umashankar, P.; Jayakrishnan, A. Evaluation of an in Situ Forming Hydrogel Wound Dressing Based on Oxidized Alginate and Gelatin. *Biomaterials* **2005**, *26*, 6335−6342.

(8) Zhu, J.; Marchant, R. E. Design Properties of Hydrogel Tissue-Engineering Scaffolds. *Expert Rev. Med. Devices* **2011**, *8*, 607−626.

(9) Vo, T. N.; Kasper, F. K.; Mikos, A. G. Strategies for Controlled Delivery of Growth Factors and Cells for Bone Regeneration. *Adv. Drug Delivery Rev.* **2012**, *64*, 1292−1309.
(10) Slaughter, B. V.; Khurshid, S. S.; Fisher, O. Z.; Khademhosseini, A.; Peppas, N. A. Hydrogels in Regenerative Medicine. *Adv. Mater.* **2009**, *21*, 3307−3329.
(11) Elbert, D. L. Liquid-Liquid Two-Phase Systems for the Production of Porous Hydrogels and Hydrogel Microspheres for Biomedical Applications: A Tutorial Review. *Acta Biomater.* **2011**, *7*, 31−56.
(12) Yang, Q.; Adrus, N.; Tomicki, F.; Ulbricht, M. Composites of Functional Polymeric Hydrogels and Porous Membranes. *J. Mater. Chem.* **2011**, *21*, 2783−2811.
(13) Annabi, N.; Nichol, J. W.; Zhong, X.; Ji, C.; Koshy, S.; Khademhosseini, A.; Dehghani, F. Controlling the Porosity and Microarchitecture of Hydrogels for Tissue Engineering. *Tissue Eng., Part B* **2010**, *16*, 371−383.
(14) Staruch, R. M. T.; Glass, G. E.; Rickard, R.; Hettiaratchy, S. P.; Butler, P. E. M. Injectable Pore-Forming Hydrogel Scaffolds for Complex Wound Tissue Engineering: Designing and Controlling Their Porosity and Mechanical Properties. *Tissue Eng., Part B* **2017**, *23*, 183−198.
(15) Wu, Y.; Chen, Y. X.; Yan, J.; Yang, S.; Dong, P.; Soman, P. Fabrication of Conductive Polyaniline Hydrogel Using Porogen Leaching and Projection Microstereolithography. *J. Mater. Chem. B* **2015**, *3*, 5352−5360.
(16) Annabi, N.; Mithieux, S. M.; Weiss, A. S.; Dehghani, F. The Fabrication of Elastin-Based Hydrogels Using High Pressure CO2. *Biomaterials* **2009**, *30*, 1−7.
(17) Ozmen, M. M.; Dinu, M. V.; Dragan, E. S.; Okay, O. Preparation of Macroporous Acrylamide-Based Hydrogels: Cryogelation under Isothermal Conditions. *J. Macromol. Sci., Part A: Pure Appl. Chem.* **2007**, *44*, 1195−1202.
(18) Kulygin, O.; Silverstein, M. S. Porous Poly(2-Hydroxyethyl Methacrylate) Hydrogels Synthesized within High Internal Phase Emulsions. *Soft Matter* **2007**, *3*, 1525−1529.
(19) Kovačič, S.; Silverstein, M. S. Hydrogels through Emulsion Templating: Sequential Polymerization and Double Networks. *Polym. Chem.* **2017**, *8*, 6319−6328.
(20) Silverstein, M. S. PolyHIPEs: Recent Advances in Emulsion-Templated Porous Polymers. *Prog. Polym. Sci.* **2014**, *39*, 199−234.
(21) Cohen, N.; Silverstein, M. S. One-Pot Emulsion-Templated Synthesis of an Elastomer-Filled Hydrogel Framework. *Macromolecules* **2012**, *45*, 1612−1621.
(22) Youssef, C.; Backov, R.; Treguer, M.; Birot, M.; Deleuze, H. Preparation of Remarkably Tough PolyHIPE Materials via Polymerization of Oil-in-Water HIPEs Involving 1-Vinyl-5-Aminotetrazole. *J. Polym. Sci., Part A: Polym. Chem.* **2010**, *48*, 2942−2947.
(23) Boyère, C.; Favrelle, A.; Léonard, A. F.; Boury, F.; Jérôme, C.; Debuigne, A. Macroporous Poly(Ionic Liquid) and Poly(Acrylamide) Monoliths from CO_2-in-Water Emulsion Templates Stabilized by Sugar-Based Surfactants. *J. Mater. Chem. A* **2013**, *1*, 8479−8487.
(24) Krajnc, P.; Štefanec, D.; Pulko, I. Acrylic Acid "Reversed" PolyHIPEs. *Macromol. Rapid Commun.* **2005**, *26*, 1289−1293.
(25) Kovačič, S.; Štefanec, D.; Krajnc, P. Highly Porous Open-Cellular Monoliths from 2-Hydroxyethyl Methacrylate Based High Internal Phase Emulsions (HIPEs): Preparation and Void Size Tuning. *Macromolecules* **2007**, *40*, 8056−8060.
(26) Kovačič, S.; Jeřabek, K.; Krajnc, P. Responsive Poly(Acrylic Acid) and Poly(*N*-Isopropylacrylamide) Monoliths by High Internal Phase Emulsion (HIPE) Templating. *Macromol. Chem. Phys.* **2011**, *212*, 2151−2158.
(27) Pahovnik, D.; Majer, J.; Žagar, E.; Kovačič, S. Synthesis of Hydrogel PolyHIPEs from Functionalized Glycidyl Methacrylate. *Polym. Chem.* **2016**, *7*, 5132−5138.
(28) Zhou, S.; Bismarck, A.; Steinke, J. H. G. Ion-Responsive Alginate Based Macroporous Injectable Hydrogel Scaffolds Prepared by Emulsion Templating. *J. Mater. Chem. B* **2013**, *1*, 4736−4745.
(29) Barbetta, A.; Dentini, M.; De Vecchis, M. S.; Filippini, P.; Formisano, G.; Caiazza, S.; Caiazza, S. Scaffolds Based on Biopolymeric Foams. *Adv. Funct. Mater.* **2005**, *15*, 118−124.
(30) Tan, H.; Tu, Z.; Jia, H.; Gou, X.; Ngai, T. Hierarchical Porous Protein Scaffold Templated from High Internal Phase Emulsion Costabilized by Gelatin and Gelatin Nanoparticles. *Langmuir* **2018**, *34*, 4820−4829.
(31) Miras, J.; Vílchez, S.; Solans, C.; Tadros, T.; Esquena, J. Kinetics of Chitosan Hydrogel Formation in High Internal Phase Oil-in-Water Emulsions (HIPEs) Using Viscoelastic Measurements. *Soft Matter* **2013**, *9*, 8678−8686.
(32) Jeon, S.-J.; Hauser, A. W.; Hayward, R. C. Shape-Morphing Materials from Stimuli-Responsive Hydrogel Hybrids. *Acc. Chem. Res.* **2017**, *50*, 161−169.
(33) Ferreira, N. N.; Ferreira, L. M. B.; Cardoso, V. M. O.; Boni, F. I.; Souza, A. L. R.; Gremião, M. P. D. Recent Advances in Smart Hydrogels for Biomedical Applications: From Self-Assembly to Functional Approaches. *Eur. Polym. J.* **2018**, *99*, 117−133.
(34) Turabee, M. H.; Thambi, T.; Duong, H. T. T.; Jeong, J. H.; Lee, D. S. A PH- and Temperature-Responsive Bioresorbable Injectable Hydrogel Based on Polypeptide Block Copolymers for the Sustained Delivery of Proteins: In Vivo. *Biomater. Sci.* **2018**, *6*, 661−671.
(35) Bazban-Shotorbani, S.; Hasani-Sadrabadi, M. M.; Karkhaneh, A.; Serpooshan, V.; Jacob, K. I.; Moshaverinia, A.; Mahmoudi, M. Revisiting Structure-Property Relationship of pH-Responsive Polymers for Drug Delivery Applications. *J. Controlled Release* **2017**, *253*, 46−63.
(36) Huang, J.; Heise, A. Stimuli Responsive Synthetic Polypeptides Derived from *N*-Carboxyanhydride (NCA) Polymerisation. *Chem. Soc. Rev.* **2013**, *42*, 7373−7390.
(37) Hadjichristidis, N.; Iatrou, H.; Pitsikalis, M.; Sakellariou, G. Synthesis of Well-Defined Polypeptide-Based Materials via the Ring-Opening Polymerization of Alpha-Amino Acid *N*-Carboxyanhydrides. *Chem. Rev.* **2009**, *109*, 5528−5578.
(38) Shen, Y.; Fu, X.; Fu, W.; Li, Z. Biodegradable Stimuli-Responsive Polypeptide Materials Prepared by Ring Opening Polymerization. *Chem. Soc. Rev.* **2015**, *44*, 612−622.
(39) Abbruzzetti, S.; Viappiani, C.; Small, J. R.; Libertini, L. J.; Small, E. W. Kinetics of Local Helix Formation in Poly-l-Glutamic Acid Studied by Time-Resolved Photoacoustics: Neutralization Reactions of Carboxylates in Aqueous Solutions and Their Relevance to the Problem of Protein Folding. *Biophys. J.* **2000**, *79*, 2714−2721.
(40) Li, G.; Wu, J.; Wang, B.; Yan, S.; Zhang, K.; Ding, J.; Yin, J. Self-Healing Supramolecular Self-Assembled Hydrogels Based on Poly(l-Glutamic Acid). *Biomacromolecules* **2015**, *16*, 3508−3518.
(41) Kokado, K.; Nagai, A.; Chujo, Y. Poly(γ-Glutamic Acid) Hydrogels with Water-Sensitive Luminescence Derived from Aggregation-Induced Emission of *o*-Carborane. *Macromolecules* **2010**, *43*, 6463−6468.
(42) Liarou, E.; Varlas, S.; Skoulas, D.; Tsimblouli, C.; Sereti, E.; Dimas, K.; Iatrou, H. Smart Polymersomes and Hydrogels from Polypeptide-Based Polymer Systems through α-Amino Acid *N*-Carboxyanhydride Ring-Opening Polymerization. From Chemistry to Biomedical Applications. *Prog. Polym. Sci.* **2018**, *83*, 28−78.
(43) Ma, G.; Lin, W.; Yuan, Z.; Wu, J.; Qian, H.; Xu, L.; Chen, S. Development of Ionic Strength/PH/Enzyme Triple-Responsive Zwitterionic Hydrogel of the Mixed l-Glutamic Acid and l-Lysine Polypeptide for Site-Specific Drug Delivery. *J. Mater. Chem. B* **2017**, *5*, 935−943.
(44) Onder, O. C.; Utroša, P.; Caserman, S.; Podobnik, M.; Žnidarič, M. T.; Grdadolnik, J.; Kovačič, S.; Žagar, E.; Pahovnik, D. Emulsion-Templated Synthetic Polypeptide Scaffolds Prepared by Ring-Opening Polymerization of *N*-Carboxyanhydrides. *Polym. Chem.* **2020**, *11*, 4260−4270.
(45) Utroša, P.; Onder, O. C.; Žagar, E.; Kovačič, S.; Pahovnik, D. Shape Memory Behavior of Emulsion-Templated Poly(ε-Caprolactone) Synthesized by Organocatalyzed Ring-Opening Polymerization. *Macromolecules* **2019**, *52*, 9291−9298.

https://doi.org/10.1021/acs.macromol.1c01490
Macromolecules 2021, 54, 8321−8330

(46) Sridhar, C. G.; Hines, W. A.; Samulski, E. T. Polypeptide Liquid Crystals: Magnetic Susceptibility, Twist Elastic Constant, Rotational Viscosity Coefficient, and Poly-γ-Benzyl-l-Glutamate Sidechain Conformation. *J. Chem. Phys.* **1974**, *61*, 947−953.
(47) Barbetta, A.; Cameron, N. R. Morphology and Surface Area of Emulsion-Derived (PolyHIPE) Solid Foams Prepared with Oil-Phase Soluble Porogenic Solvents: Three-Component Surfactant System. *Macromolecules* **2004**, *37*, 3202−3213.
(48) Shirbin, S. J.; Karimi, F.; Chan, N. J.-A.; Heath, D. E.; Qiao, G. G. Macroporous Hydrogels Composed Entirely of Synthetic Polypeptides: Biocompatible and Enzyme Biodegradable 3D Cellular Scaffolds. *Biomacromolecules* **2016**, *17*, 2981−2991.
(49) Sulistio, A.; Blencowe, A.; Wang, J.; Bryant, G.; Zhang, X.; Qiao, G. G. Stabilization of Peptide-Based Vesicles via in Situ Oxygen-Mediated Cross-Linking. *Macromol. Biosci.* **2012**, *12*, 1220−1231.
(50) Hayashi, T.; Tabata, Y.; Nakajima, A. Biodegradation of Poly(α-Amino Acid) in Vitro. *Polym. J.* **1985**, *17*, 463−471.
(51) Rao, J.; Zhang, Y.; Zhang, J.; Liu, S. Facile Preparation of Well-Defined AB_2 Y-Shaped Miktoarm Star Polypeptide Copolymer via the Combination of Ring-Opening Polymerization and Click Chemistry. *Biomacromolecules* **2008**, *9*, 2586−2593.
(52) Gil, E. S.; Hudson, S. Stimuli-Reponsive Polymers and Their Bioconjugates. *Prog. Polym. Sci.* **2004**, *29*, 1173−1222.
(53) Onder, O. C.; Yilgor, E.; Yilgor, I. Preparation of Monolithic Polycaprolactone Foams with Controlled Morphology. *Polymer* **2018**, *136*, 166−178.
(54) Ovadia, M.; Silverstein, M. S. High Porosity, Responsive Hydrogel Copolymers from Emulsion Templating. *Polym. Int.* **2016**, *65*, 280−289.
(55) Sun, J.-Y.; Zhao, X.; Illeperuma, W. R. K.; Chaudhuri, O.; Oh, K. H.; Mooney, D. J.; Vlassak, J. J.; Suo, Z. Highly Stretchable and Tough Hydrogels. *Nature* **2012**, *489*, 133−136.
(56) Zhang, T.; Silverstein, M. S. Doubly-Crosslinked, Emulsion-Templated Hydrogels through Reversible Metal Coordination. *Polymer* **2017**, *126*, 386−394.
(57) Bui, H. L.; Huang, C.-J. Tough Polyelectrolyte Hydrogels with Antimicrobial Property via Incorporation of Natural Multivalent Phytic Acid. *Polymers* **2019**, *11*, 1721−1740.
(58) Sun, T. L.; Kurokawa, T.; Kuroda, S.; Ihsan, A. B.; Akasaki, T.; Sato, K.; Haque, M. A.; Nakajima, T.; Gong, J. P. Physical Hydrogels Composed of Polyampholytes Demonstrate High Toughness and Viscoelasticity. *Nat. Mater.* **2013**, *12*, 932−937.
(59) Blackman, L. D.; Gunatillake, P. A.; Cass, P.; Locock, K. E. S. An Introduction to Zwitterionic Polymer Behavior and Applications in Solution and at Surfaces. *Chem. Soc. Rev.* **2019**, *48*, 757−770.
(60) Zhang, T.; Silverstein, M. S. Highly porous, emulsion-templated, zwitterionic hydrogels: amplified and accelerated uptakes with enhanced environmental sensitivity. *Polym. Chem.* **2018**, *9*, 3479−3487.
(61) Yue, Y.; Wang, X.; Han, J.; Yu, L.; Chen, J.; Wu, Q.; Jiang, J. Effects of Nanocellulose on Sodium Alginate/Polyacrylamide Hydrogel: Mechanical Properties and Adsorption-Desorption Capacities. *Carbohydr. Polym.* **2019**, *206*, 289−301.
(62) Kraut, J. Chymotrypsin-Chemical Properties and Catalysis. *Enzymes* **1971**, *3*, 213−248.
(63) Johnson, P.; Smillie, L. B. The Amino Acid Sequence and Predicted Structure of Streptomyces Griseus Protease A. *FEBS Lett.* **1974**, *47*, 1−6.
(64) Jurásek, L.; Carpenter, M. R.; Smillie, L. B.; Gertler, A.; Levy, S.; Ericsson, L. H. Amino Acid Sequence of Streptomyces Griseus Protease B, a Major Component of Pronase. *Biochem. Biophys. Res. Commun.* **1974**, *61*, 1095−1100.
(65) Xin, X.; Wu, J.; Zheng, A.; Jiao, D.; Liu, Y.; Cao, L.; Jiang, X. Delivery Vehicle of Muscle-Derived Irisin Based on Silk/Calcium Silicate/Sodium Alginate Composite Scaffold for Bone Regeneration. *Int. J. Nanomed.* **2019**, *14*, 1451−1467.
(66) Hasturk, O.; Jordan, K. E.; Choi, J.; Kaplan, D. L. Enzymatically Crosslinked Silk and Silk-Gelatin Hydrogels with Tunable Gelation Kinetics, Mechanical Properties and Bioactivity for Cell Culture and Encapsulation. *Biomaterials* **2020**, *232*, 119720.

https://doi.org/10.1021/acs.macromol.1c01490
Macromolecules 2021, 54, 8321−8330